A flexible anisotropic magnetoresistance sensor for magnetic field detection

Jie Chen[1],* and Zhongjin Zhang[1]

[1] Key Laboratory of MEMS of Ministry of Education, Southeast University, Si-Pai-Lou 2, Nanjing 210096, China

ABSTRACT

Anisotropic magnetoresistance (AMR) sensors with a flexible substrate are presented in this paper. The AMR sensors were fabricated on polyimide (PI) material in a surface micromachining process, and the minimum linewidth of the sensors was reduced to 3 μm by optimization of the process. An orthogonal-arranged Wheatstone bridge structure was proposed to improve the voltage output, and the AMR strips in series–parallel connection were designed to improve the sensitivity. The AMR sensors with Wheatstone bridge show high linearity, sensitivity, and voltage output performance by measurement. A maximum Wheatstone bridge voltage output of about 0.07 mV was achieved for 0.5 V bias in the magnetic field of 100 Gs, and the sensitivity value of about 1.5 Gs^{-1} was obtained. Moreover, the AMR sensors had good robustness upon mechanical bending, and a maximum bend radius of about 2.3 cm was achieved. The research results demonstrated the feasibility of manufacturing high-performance small-sized AMR sensors on flexible substrates and showed great potential for magnetic field detection in non-planar applications.

1 Introduction

Flexible sensors are in great demand in various applications, e.g., consumer electronics, entertainment, automotive, industrial, and healthcare in recent years [1]. Organic polymer materials as flexible substrates have been widely used in flexible sensors due to the characteristics of high consistency, ductility, bendability, and lightweight [2]. Flexible sensors can achieve conformal contact on human skin or curved surfaces, thus making it possible for miniaturization and integration [3]. Magnetic field sensors based on the magnetoresistance (MR) effect have attracted increasing massive attention over the last decades and have made a significant contribution to a variety of industrial fields, such as automobiles, aerospace fields, and storage technology [4]. Candid Reig [5] and his group focused on giant magnetoresistance (GMR) sensors in electrical current sensing applications and reviewed the research progress of GMR sensors. Linear magnetoresistance in Pt/FePt/ZnO/Fe/Pt multilayer magnetic sensor which achieved a large linear range from + 5 kOe to − 5 kOe and MR value of 1.2% was investigated by Liu [6]. The properties of AMR sensors with the Wheatstone bridge were studied by Demirci [7], and the

sensitivity of 0.55 Oe^{-1} was got in the AMR sensor research. Zheng [8] fabricated the organic spin valve devices with multilayer magnetic materials utilizing donor–acceptor conjugated polymer as the spacer, and the polymer contributed a negative MR response was observed. Flexible magnetic materials and sensors have also been drawing increasing scientific interest due to their prospective applications. Meanwhile, the fabrication of flexible magnetic sensors has been possible based on numerous researches on rigid magnetic sensors. The group of Jana [9] reviewed the methods of fabricating flexible multiferroic films and the properties of multiferroic thin films on flexible substrates, and the great potential of flexible multiferroic films in wearable devices was shown in their review. Gaspar [10] reported magnetic tunnel junction (MTJ) sensing devices with magnetoresistance responses on flexible substrates, whose performance was fully in line with those from rigid substrates. A flexible GMR device with a strain-sensitive ferromagnetic Co layer and a strain-insensitive NiFe layer was fabricated [11]. A kind of printable sensor based on AMR fakes of permalloy was investigated [12] by Eduardo, and the AMR value of this sensor was 0.34% in the field of 400 mT.

Henriksen [13] and his group proposed that the sensitivity of planar Hall effect bridge (PHEB) sensors can be enhanced in proportion to the effective AMR branch length L_{eff}, which is expressed as

$$L_{eff} = (n \times l)/w \tag{1}$$

where n is the number of AMR strips, w is the width of the strips, and l is the length of the strips. Increasing the L_{eff} of AMR sensor bridges is a way to improve the sensitivity of the AMR sensor. However, the resistance increases as the effective length increases, resulting in thermal noise [14, 15]. The surface roughness of the substrate also has an impact on the microstructure of the material due to existing internal thermal stress and inherent stress caused by crystal defects [16]. To achieve the same performance as the silicon-based sensor, the sensor with a flexible substrate needs to be optimized.

In this work, a series of flexible AMR sensors were designed and fabricated with ferromagnetic by micromachining, whose AMR effect has been characterized. Flexible organic materials with good smoothness and AMR material with good magnetic performance were used to improve the AMR effect of the ferromagnetic film on the flexible substrate.

Series–parallel AMR strips maintaining the large L_{eff} were proposed to reduce thermal noise and improve the sensitivity of the AMR sensor. Meanwhile, an orthogonal-arranged bridge structure, which is different from the sensor structures proposed by Demirci [7] and Wang [17], was designed to achieve a high voltage output and a wide linear range. The sensors with the minimum line width of 3 μm were achieved by optimizing the micromachining process. Compared to Eduardo [12] and Wang [17], the minimum line width of AMR sensors fabricated on flexible substrates was reduced by more than 5 times. The sensors were tested, and the performance of the small-size sensors was similar to that of the large-size sensors.

2 Theory and design

Magnetic field sensors based on the AMR effect were developed to achieve high linearity and sensitivity in this paper. Permalloy ($Ni_{80}Fe_{20}$) with the AMR effect [18, 19] was chosen to be the function material of the magnetic field sensors. The AMR effect, that the longitudinal resistivity of a ferromagnetic metal depends on the orientation of its magnetization concerning the applied electric field direction, was discovered by William Thomson in 1857 [20]. When the current density is parallel to the magnetization, magnetic resistance has a value of $R_{\parallel}$, and $R_{\perp}$ for the perpendicular case. The AMR ratio [21] is expressed as

$$AMR = (R_{\parallel} - R_{\perp})/R_{\perp} \tag{2}$$

As shown in Fig. 1, four AMR sensors with Wheatstone bridge in different combinations were proposed to improve the performance. The adjacent bridges were parallel-arranged shown in Fig. 1a, b, and those were orthogonal-arranged shown in Fig. 1c, d. The use of the Wheatstone bridge structure was aimed at offsetting the thermal noise, and orthogonal arrangement played a significant role in improving voltage output performance. The orthogonal-arranged sensor has better voltage output than the parallel-arranged one at the same voltage bias theoretically, since the orthogonal-arranged one has a larger AMR difference between adjacent bridges. Meanwhile, the AMR strips in series–parallel connection in Fig. 1c, d were applied to reduce the thermal noise caused by resistance increase,

Fig. 1 The AMR sensors in Wheatstone bridge structure. **a** The parallel-arranged bridge structure with the strips in a series connection. **b** The parallel-arranged bridge structure with the strips in a series–parallel connection. **c** The orthogonal-arranged bridge structure with the strips in a series connection. **d** The orthogonal-arranged bridge structure with the strips in a series–parallel connection
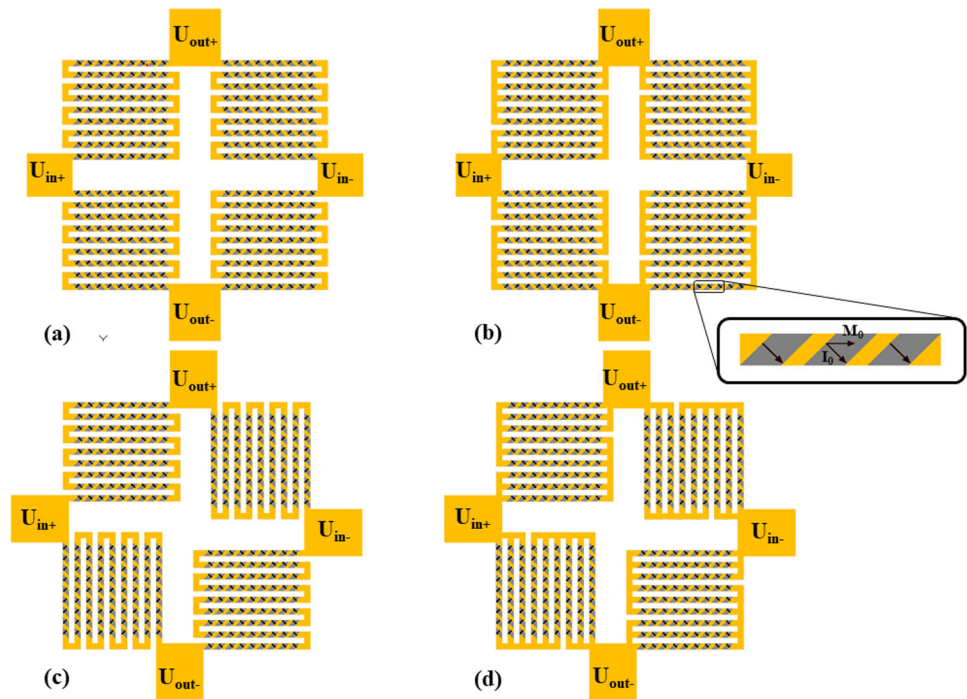
compared with the series strips in Fig. 1a, b. The geometry of every AMR strip with $w = 5$ μm, $l = 100$ μm, and $n = 9$ was designed, and adjacent strips had a distance of 5 μm. With the same L_{eff}, the equivalent resistance of the series–parallel structure is only 1/9 of that of the series structure. Barber pole electrodes at 45° or 135° to the magnetic axis were used to make the voltage output of the AMR sensor change linearly with the external magnetic field. As shown in Fig. 1b, the current I_0 is 45° or 135° to the magnetic domain M_0 when the AMR strip is covered with barber poles. Barber poles had a width of 3 μm, and the distance between two barber poles was 3.5 μm.

Most flexible substrates with low surface flatness have a certain loss on the AMR effect of ferromagnetic film compared with silicon substrates [16]. Therefore, PI which has the advantages of a large thermal expansion coefficient, good chemical resistance, and high insulation was used as a flexible substrate to reduce the influence of surface roughness on the AMR effect. In addition, tantalum (Ta) was deposited onto the PI surface as a buffer layer to reduce surface roughness and surface stress of $Ni_{80}Fe_{20}$ film.

3 Fabrication process and experiment

The AMR sensors with a Wheatstone bridge were prepared by using magnetron-sputter and microlithography deposition techniques. The substrate® (Wuxi Alflex Optoelectronic Tech Companies., LTD), a glass coated with PI, was cut into 7×7 cm^2 squares to be compatible with the standard micromachining process. Then, the substrate was sequentially cleaned with an ultrasound-assisted procedure in acetone, alcohol, and deionized water. The process flow is shown schematically in Fig. 2.

In step (a), thin films of Ta (5 nm) and $Ni_{80}Fe_{20}$ (60 nm) layers were grown on PI substrate by ion beam sputtering. Ta film served as the buffer layer, and $Ni_{80}Fe_{20}$ film was the functional layer. The deposition rate of Ta was 3.82 nm/min, and the rate of $Ni_{80}Fe_{20}$ was 6.73 nm/min. The base pressure was 5×10^{-4} Pa. The Ar sputter pressure was 0.4 Pa. In steps (b) and (c), the patterning of AMR strip structures was realized on Ta/$Ni_{80}Fe_{20}$ films by photolithography and ion beam etching in turn. To avoid the curl of PI foil caused by high temperature, positive adhesive and dark field masks were used in all lithography processes. Barber poles and pads were deposited on the MR strips by a lift-off process. In step (d), the substrate was spin-coated with photoresist as a sacrificial layer and patterned by

Fig. 2 Manufacturing process of flexible AMR sensors. **a** Magnetron sputtering of Ta and $Ni_{80}Fe_{20}$. **b** First lithography. **c** Dry etching. **d** Second lithography. **e** Evaporation of Ti and Au. **f** dissolution of photoresist
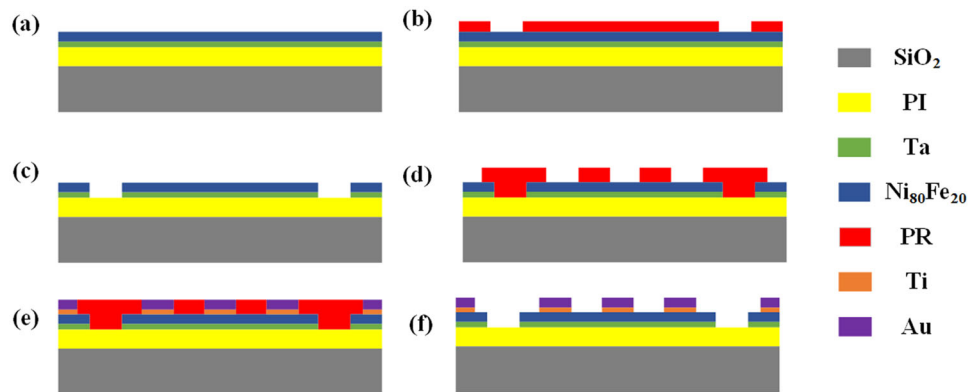
photolithography. In step (e), Ti (10 nm) and Au (80 nm) films were grown on a patterned substrate by the thermal evaporator. In step (f), the photoresist was dissolved in an acetone bath. Finally, the PI layer was separated from the glass substrate. The flexible AMR sensor separated from the glass plate is shown in Fig. 3. The high-res images of the AMR sensors captured by a scanning electron microscope (SEM) are shown in Fig. 4. The $Ni_{80}Fe_{20}$ film had good adhesion on the PI surface and surface smoothness due to the Ta buffer layer.

A Helmholtz coil driven by a typical current served as a magnetic field source. A bare AMR strip was used to characterize the AMR effect of $Ni_{80}Fe_{20}$ film fabricated on the PI substrate. The AMR ratio of the bare strip was measured using typical four points probe resistivity with the magnetic field intensity of -100 Gs to 100 Gs.

As shown in Fig. 5a, $R_{\parallel}$ and $R_{\perp}$ tend to be saturated under a magnetic field of 85 Gs, and the AMR ratio reaches the maximum value of 0.52%. The AMR ratio on PI substrate is reduced by about 0.65% compared to the one of 1.17% on silicon substrate measured by Wang [17]. The decrease in the AMR ratio is due to
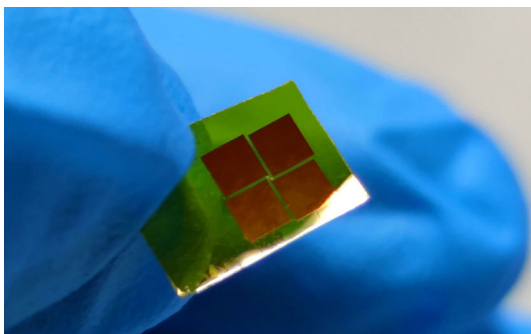

Fig. 3 The flexible AMR sensor separated from the glass substrate

the larger surface roughness of PI film. As shown in Fig. 5a, the magnetic resistance has good linearity in the range of − 30 Gs and 30 Gs. Apart from the AMR ratio measurements, the sensitivity [22] of the bare strip was calculated, which was expressed as

$$S = \frac{dR(H_{\text{ext}})/dH_{\text{ext}}}{R(H_{\text{ext}})} \quad (3)$$

where H_{ext} is the magnetic field intensity, $R(H_{\text{ext}})$ is the resistance value of AMR under H_{ext}. Figure 5b represents that the sensitivity of the AMR bare strip was 1.2 Gs^{-1}.

Barber poles were added to the flexible AMR sensors, and four AMR strips of the sample in Fig. 4a were tested. As shown in Fig. 6, these strips, respectively, have an AMR ratio of about 0.42%, 0.35%, 0.27%, and 0.4% for the AMR ratio of the strips. The AMR ratio deviation is generated due to the barber poles, compared to 0.52% of the bare strip. Besides, the strips with 45° barber poles have a higher AMR ratio than the ones with 135° barber poles due to opposite transverse current components. The difference was utilized to increase the AMR ratio by using a Wheatstone bridge structure.

A typical voltage source was used to supply 0.5 V voltage to drive the Wheatstone bridge. The voltage outputs of the AMR sensors in Fig. 4 were measured under the magnetic field between − 100 Gs and 100 Gs with a digital multimeter. As shown in Fig. 7a, the voltage output of sensor A has a linear variation between − 30 Gs and 30 Gs, and a linear range for sensor B from − 20 Gs to 20 Gs has been observed. Both sensor A and B have great linearity, while the linear range of sensor A is wider than that of sensor B. The voltage outputs for sensors A and B are about 0.03 mV near the magnetic field of 30 Gs and 20 Gs, respectively. The voltage outputs in Fig. 7b, which
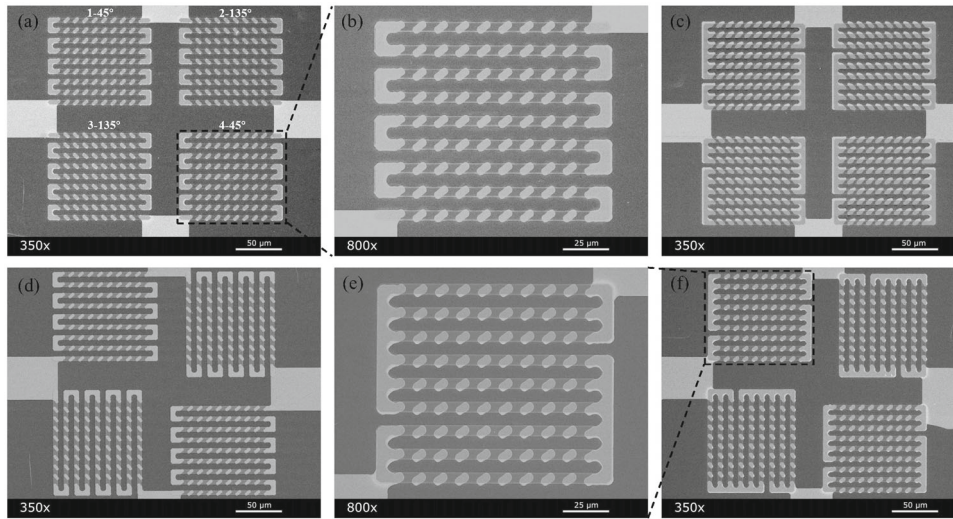
Fig. 4 High-res SEM images of flexible AMR sensors. **a** Sensor A: Parallel-arranged AMR sensor with series strips. **b** Enlarged AMR strips in series connection with barber poles. **c** Sensor B: Parallel-arranged AMR sensor with series–parallel strips. **d** Sensor C: Orthogonal-arranged sensors with series strips. **e** Enlarged AMR strips in series–parallel connection with barber poles. **f** Sensor D: Orthogonal-arranged sensors with series–parallel strips

Fig. 5 The characterization of AMR effect. **a** The AMR ratio of the bare AMR strip. **b** The sensitivity of the bare AMR strip
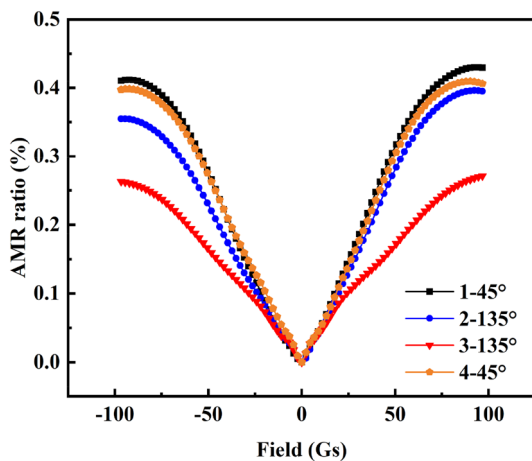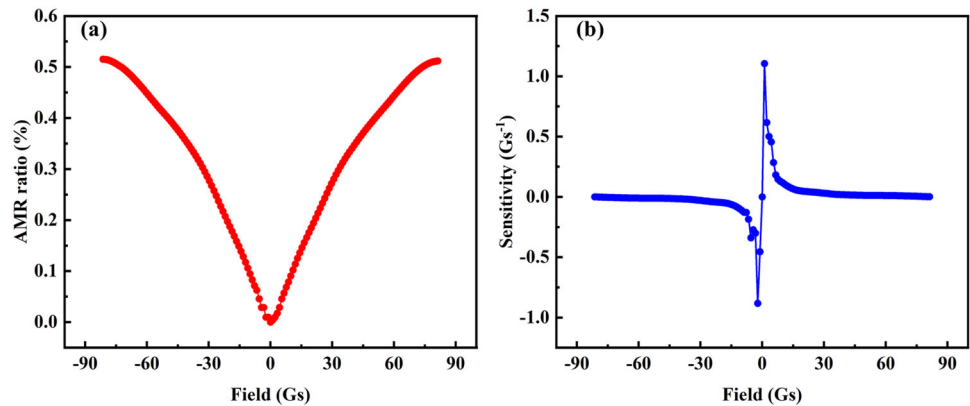

Fig. 6 The AMR ratio of the four AMR strips in the Wheatstone bridge

are 0.05 mV for sensor C and 0.08 mV for sensor D, are increased by a factor of about 2–3 compared to sensors A and B. By comparison of Fig. 7a, b, sensor C and D also have high linearity before the magnetic resistance tends to saturation and have wider linear range than sensor A and B. Depicted in Fig. 7c, d, four sensors, respectively, have the sensitivity of about 1.3, 1.5, 0.91 and 0.92 Gs^{-1}, and the results are better than 0.6 Gs^{-1} got by E. Demirci [7]. Sensors B and D in series–parallel connections have better sensitivity than sensors A and C. The sensitivity was improved by the reduction of the resistance in the Wheatstone bridge. Sensors B and D have smaller equivalent resistance than sensors A and C, although they have the same number of strips. Hence, sensors B and D are more sensitive to the magnetic field than

Fig. 7 The voltage output of the AMR sensor with magnetic field intensity. **a** The voltage output of sensor A and B. **b** The voltage output of sensor C and D. **c** The sensitivity of sensor A and B. **d** The sensitivity of sensor C and D
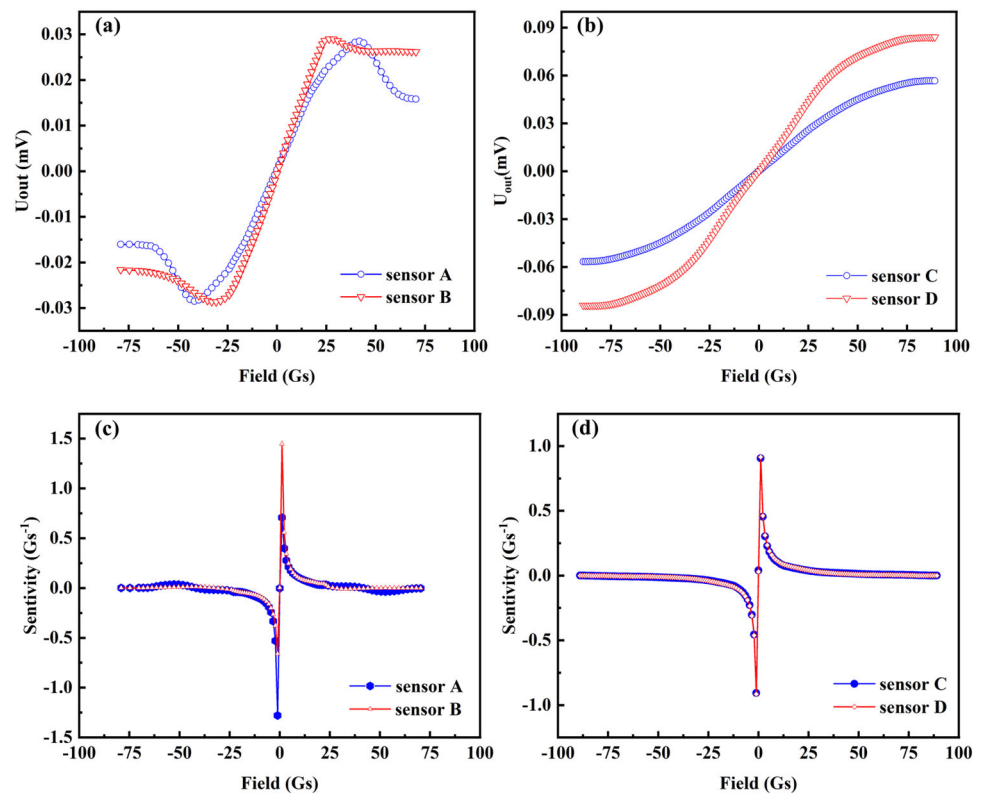

sensors A and C under the same magnetic field. Besides, the design that adjacent bridges were orthogonal-arranged in a Wheatstone bridge, such as sensors C and D, significantly improved the voltage output and linearity of the flexible AMR sensor. Meanwhile, it can be observed that sensors A and B with parallel-arranged bridges have better sensitivity.

The performance of the AMR sensors with different bending curvatures is an important indicator of a flexible magnetic field sensor. The AMR sensor was attached to the surface of cylinders with different bending curvatures, and the resistance value of four bridges was measured with an ohmmeter. As shown in Fig. 8a, the resistance value change of the four AMR strips in sensor A under different bending curvatures. In addition, the bigger the bending angle of the sensor, the bigger the resistance value of the strip. Then, the voltage output of the sensor was measured in different bent states as shown in Fig. 8b. With the increase of bending curvature, the voltage output of the sensor becomes smaller and smaller, and the performance decreases gradually. In a bent state, there was a performance loss or even an invalid for the flexible AMR sensors caused by the internal stress generated by the deformation of $Ni_{80}Fe_{20}$ film.

4 Conclusion

In summary, the flexible AMR sensors with good linearity or sensitivity have been manufactured on the PI substrate. By optimizing the micromachining process, small-size sensors which had a minimum line width of about 3 µm on the PI film were achieved. The AMR ratio on PI substrate of about 0.52% was measured. The performance of the AMR sensor was improved in this paper by optimization of the structure. The sensitivity was improved by using the arrangement of AMR strips in a series–parallel connection to reduce the resistance, and the sensitivity of sensor B was raised to 1.5 Gs^{-1}. The use of barber poles achieved a self-bias in the Wheatstone bridge AMR sensor to generate linear voltage output. The AMR sensor in an orthogonal-arranged structure had high linearity and better voltage output performance. A wide linear range from − 35 Gs to 35 Gs was measured in sensor C. And the voltage output of sensor D, which was approximately 0.08 mV, was increased by a factor of 2.7 compared to sensor B under 0.5 V voltage driving. Power consumption was decreased when getting the same output performance. The maximum bend radius of about 2.3 cm

Fig. 8 The performance of AMR sensor in bending state. **a** The change of resistance in different bending radii. **b** The maximum output of the AMR sensor in different bending radii
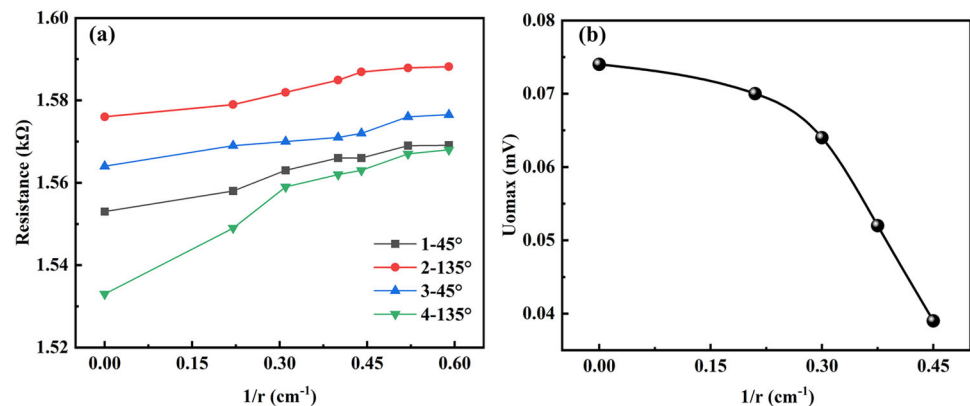
was achieved, and the maximum output voltage was approximately half of the flat state.

Author contributions

All authors contributed to the study conception and design. Material preparation, data collection and analysis were performed by JC and ZZ. The first draft of the manuscript was written by JC and all authors commented on previous versions of the manuscript. All authors read and approved the final manuscript.

Data availability

The data that support the findings of this study are available from the corresponding author upon reasonable request.

Declarations

Conflict of interest The authors have not disclosed any competing interests.

Ethical approval This article does not contain any studies with human participants or animals performed by any of the authors. The authors declare no competing interests.

References

1. J.T. Yu, L. Sun, Y. Xiao, S.W. Jiang, W.L. Zhang, Electron. Compon. Mater. **38**, 6 (2019)
2. Y.H. Chai, Y.X. Guo, W. Bian, W. Li, T. Yang, M.D. Yi, Q.L. Fan, L.H. Xie, W. Huang, Acta Phys. Sin. **63**, 2 (2014). https://doi.org/10.7498/aps.63.027302
3. G.Z. Shen, Prog. Nat. Sci. **31**, 6 (2021). https://doi.org/10.1016/j.pnsc.2021.10.005
4. L. Jogschies, D. Klaas, R. Kruppe, J. Rittinger, P. Taptimthong, A. Wienecke, L. Rissing, M.C. Wurz, Sensors **15**, 11 (2015). https://doi.org/10.3390/s151128665
5. C. Reig, M.D. Cubells-Beltran, D.R. Munoz, Sensors **9**, 10 (2009). https://doi.org/10.3390/s91007919
6. X. Liu, Z.L. Song, R. Wang, Z.Y. Quan, Adv. Condens. Matter Phys. (2016). https://doi.org/10.1155/2016/8528617
7. E. Demirci, J. Supercond. Nov. Magn. **33**, 12 (2020). https://doi.org/10.1007/s10948-020-05646-4
8. N.H. Zheng, X. Wang, Y.H. Zheng, D. Li, Z.Z. Lin, W.F. Zhang, K.J. Jin, G. Yu, Adv. Mater. Interfaces **7**, 18 (2020). https://doi.org/10.1002/admi.202000868
9. B. Jana, K. Ghosh, K. Rudrapal, P. Gaur, P.K. Shihabudeen, A.R. Chaudhuri, Front. Phys. (2022). https://doi.org/10.3389/fphy.2021.822005

10. J. Gaspar, H. Fonseca, E. Paz, M. Martins, J. Valadeiro, S. Cardoso, R. Ferreira, P.P. Freitas, IEEE Trans. Magn. **53**, 4 (2017). https://doi.org/10.1109/TMAG.2016.2623669

11. S. Ota, A. Ando, D. Chiba, Nat. Electron. **1**, 2 (2018). https://doi.org/10.1038/s41928-018-0022-3

12. E.S.O. Mata, G.S.C. Bermudez, M. Ha, T. Kosub, Y. Zabila, J. Fassbender, D. Makarov, Appl. Phys. A **127**, 4 (2021). https://doi.org/10.1007/s00339-021-04411-1

13. A. Persson, R.S. Bejhed, H. Nguyen, K. Gunnarsson, B.T. Dalslet, F.W. Osterberg, M.F. Hansen, P. Svedlindh, Sens. Actuator A **171**, 2 (2011). https://doi.org/10.1016/j.sna.2011.09.014

14. C.Y. Wang, W. Su, Z.Q. Hu, J.T. Pu, M.M. Guan, B. Peng, L. Li, W. Ren, Z.Y. Zhou, Z.D. Jiang, M. Liu, IEEE Trans. Magn. **54**, 11 (2018). https://doi.org/10.1109/TMAG.2018.2846758

15. L.J. Wang, J. Univ. Sci. Technol. Beijing **28**, 8 (2006)

16. A. Bedoya-Pinto, M. Donolato, M. Gobbi, L.E. Hueso, P. Vavassori, Appl. Phys. Lett. **104**, 6 (2014). https://doi.org/10.1063/1.4865201

17. Z.G. Wang, X.J. Wang, M.H. Li, Y. Gao, Z.Q. Hu, T.X. Nan, X.F. Liang, H.H. Chen, J. Yang, S. Cash, N.X. Sun, Adv. Mater. **28**, 42 (2016). https://doi.org/10.1002/adma.201602910

18. C.H. Lai, H. Matsuyama, R.L. White, T.C. Anthony, IEEE Trans. Magn. **31**, 6 (1995). https://doi.org/10.1109/20.490068

19. Y. Saito, K. Inomata, K. Yusu, A. Goto, H. Yasuoka, Phys. Rev. B **52**, 9 (1995). https://doi.org/10.1103/PhysRevB.52.6500

20. W. Thomson, Proc. R. Soc. Lond. (1876). https://doi.org/10.1098/rstl.1876.0026

21. J. Neamtu, M. Volmer, A. Coraci, IEEE (1998). https://doi.org/10.1109/SMICND.1998.732348

22. J. Mouchot, P. Gerard, B. Rodmacq, IEEE Trans. Magn. **29**, 6 (1993). https://doi.org/10.1109/20.280928